Unclassified

(1)

AD-A211 358 REPORT DOCUMENTATION PAGE

DTIC ELECTE AUG 16 1989 S D

1b. RESTRICTIVE MARKINGS THIS FILE COPY

2a. SECURITY CLASSIFICATION AUTHORITY

3. DISTRIBUTION/AVAILABILITY OF REPORT
Approved for public release; Distribution unlimited

2b. DECLASSIFICATION/DOWNGRADING SCHEDULE

4. PERFORMING ORGANIZATION REPORT NUMBER(S)
GL-TR-89-0200

5. MONITORING ORGANIZATION REPORT NUMBER(S)

6a. NAME OF PERFORMING ORGANIZATION
Geophysics Laboratory

6b. OFFICE SYMBOL (If applicable)
LIU

7a. NAME OF MONITORING ORGANIZATION

6c. ADDRESS (City, State, and ZIP Code)
Hanscom AFB
Massachusetts 01731-5000

7b. ADDRESS (City, State, and ZIP Code)

8a. NAME OF FUNDING/SPONSORING ORGANIZATION

8b. OFFICE SYMBOL (If applicable)

9. PROCUREMENT INSTRUMENT IDENTIFICATION NUMBER

8c. ADDRESS (City, State, and ZIP Code)

10. SOURCE OF FUNDING NUMBERS

PROGRAM ELEMENT NO.	PROJECT NO.	TASK NO.	WORK UNIT ACCESSION NO
63220C	S321	06	03

11. TITLE (Include Security Classification)
Spatial Characteristics of Airglow and Solar Scatter Radiance from the Earth's Atmosphere

12. PERSONAL AUTHOR(S)
R. Huguenin*, R. Wohlers*, M. Weinberg*, R. Huffman, R. Fastes, F. DelGreco

13a. TYPE OF REPORT	13b. TIME COVERED	14. DATE OF REPORT (Year, Month, Day)	15. PAGE COUNT
Reprint	FROM _____ TO _____	1989 August 9	12

16. SUPPLEMENTARY NOTATION *Aerodyne Research, Inc., 45 Manning Road, Billerica, MA 01821
~~Reprinted from SPIE, Paper No. 1158-02~~

17. COSATI CODES		
FIELD	GROUP	SUB-GROUP

18. SUBJECT TERMS (Continue on reverse if necessary and identify by block number)
Airglow; Solar Scatter; Ultraviolet spatial structure, Reprints, (jhd)

19. ABSTRACT (Continue on reverse if necessary and identify by block number)

Data measured by the Polar BEAR/AIRS UV Imager Experiment were processed to extract spatial radiance characteristics. Photometer mode 1304 Å dayside data measured on Julian Day 219, 1987, near mid-day were analyzed. The spatial structure of thermospheric dayside radiance at 1304Å appeared to be controlled principally by turbulence over spatial scales of [illegible] meters, with modifications imposed by Rayleigh scattering effects and magnetospherically forced phenomena. Spatial structure can be adequately modeled fractally, using dimensions based on Kolmogorov formalism modified by the Rayleigh scattering phase function. Mean radiance can be modeled using existing models of radiant intensity, resonance scattering, and absorption combined with thermospheric composition and general circulation models, such as MSIS-83, scaled to the mean and RMS intensities measured by Polar BEAR. The results can be incorporated in a background radiance simulation model that will provide a means for testing and refining phenomenological models of the structured earth background. This will be important not only for improving physical and chemical models of atmospheric features and processes, but it will allow parametric predictions of spatial structure and clutter to be developed for sensor modeling applications.

20. DISTRIBUTION/AVAILABILITY OF ABSTRACT	21. ABSTRACT SECURITY CLASSIFICATION
☐ UNCLASSIFIED/UNLIMITED ☒ SAME AS RPT. ☐ DTIC USERS	Unclassified

22a. NAME OF RESPONSIBLE INDIVIDUAL	22b. TELEPHONE (Include Area Code)	22c. OFFICE SYMBOL
Francis DelGreco	(617) 377-4758	LIU

DD FORM 1473, 84 MAR 83 APR edition may be used until exhausted. All other editions are obsolete.

SECURITY CLASSIFICATION OF THIS PAGE Unclassified

89 8 16 031

Spatial characteristics of airglow and solar scatter radiance from the Earth's atmosphere

R. Huguenin, R. Wohlers and M. Weinberg
Aerodyne Research, Inc.
45 Manning Road
Billerica, MA 01821

and

R. Huffman, R. Eastes, and F. Delgreco
Air Force Geophysics Laboratory
Hanscom, AFB, MA 01731

ABSTRACT

Data measured by the Polar BEAR/AIRS UV Imager Experiment were processed to extract spatial radiance characteristics. Photometer mode 1304 Å dayside data measured on Julian Day 219, 1987, near mid-day were analyzed. The spatial structure of thermospheric dayside radiance at 1304Å appeared to be controlled principally by turbulence over spatial scales of 10^7 - 10^2 meters, with modifications imposed by Rayleigh scattering effects and magnetospherically forced phenomena. Spatial structure can be adequately modeled fractally, using dimensions based on Kolmogorov formalism modified by the Rayleigh scattering phase function. Mean radiance can be modeled using existing models of radiant intensity, resonance scattering, and absorption combined with thermospheric composition and general circulation models, such as MSIS-83, scaled to the mean and RMS intensities measured by Polar BEAR. The results can be incorporated in a background radiance simulation model that will provide a means for testing and refining phenomenological models of the structured earth background. This will be important not only for improving physical and chemical models of atmospheric features and processes, but it will allow parametric predictions of spatial structure and clutter to be developed for sensor modeling applications.

1. INTRODUCTION

Information about the spatial characteristics of ultraviolet radiation from the Earth's atmosphere is important to both the atmospheric research and sensor modeling communities. Such information provides important constraints on a broad range of models of physical and chemical processes in the atmosphere.

Reliability testing and refinement of the basic phenomenological models is becoming critical for accurate prediction models. Spacecraft measurements of background phenomena and clutter are necessarily restricted with respect to the ranges of conditions that can be sampled. Clutter prediction models are consequently needed to interpolate and extrapolate existing measurements to the other conditions that may be encountered. Needed accuracy of the clutter predictions require that models be based on accurate and reliable phenomenological models.

In this paper we report the first set of results from an effort to derive information about the spatial characteristics of the structured ultraviolet Earth

background. Polar BEAR/AIRS Ultraviolet Imager Experiment photometer mode data were analyzed to extract information about dayside thermospheric radiance. Thermospheric radiance was selected because it has been relatively extensively studied and parametrically modeled, providing a good foundation for the development of a spatial structure model. Data were restricted to nadir-viewing geometry. Emphasis in this paper is on derivation of spatial structure and the phenomenology controlling it. In a companion paper spatial clutter characteristics of the thermosphere are modeled based on the spatial structure information derived here.[1]

Polar BEAR/AIRS UV Imager

The AIRS UV Imager experiment has been measuring aurora and airglow data from a nearly circular, non-sun synchronous, polar, 1000 km elevation orbit since December 1986. The instrument is mounted in an earth nadir-viewing direction on the Polar BEAR Satellite, a Navy Transit class satellite that is a 3-axis passively stabilized platform with a momentum wheel. The sensor can operate in either a multispectral imaging, nadir spectroscopy, or multispectral nadir photometry mode, selectable by ground command. The photometer mode data was processed to extract spatial clutter information. In the photometer mode the AIRS UV Imager is in a fixed nadir viewing orientation. The sensor's field-of-view (5 km across track x 20 km along track IFOV) moves along the ground track at a rate of 6.37 km s^{-1}. Measurements are made with an integration period of 6.8330 ms, during which the IFOV slides ~43.5 meters along the ground track.

Data Processing

To derive the spatial characteristics of the background scene radiance, the data were processed into power spectral density. From the power spectral density (PSD) relevant spatial characteristics of the background radiance can be derived. The logarithmic slope (β) of the PSD is directly related to fractal dimension of the background radiance pattern, so that the geometric characteristics of radiance patterns can be described and related to phenomenological models. In particular, for one-dimensional data[2]

$$\beta = 2H + 1 = 3 - 2\,(D - E) \qquad (1)$$

where

D = self similar fractal dimension

H = self affine fractal dimension

E = Euclidean dimension

Data for multiple station passes were processed into normalized power spectral density for station passes of 303 second duration each (2020 km length). Normalization was to the zero spatial frequency value. Each station pass was processed into two or three normalized power spectral densities, depending on the length of the station pass. A total of 15 PSDs were generated from the six passes of 1304 Å data. The 15 PSD's were averaged to reduce noise. The resultant average PSD is shown in Figure 1. At the higher spatial frequencies the PSD is noisy and it appears to be totally uncorrelated with spatial frequency, i.e., the

log-log plot has approximately zero slope. At the lower spatial frequencies, noise levels are lower and the PSD appears to be highly correlated with spatial frequency, i.e., the log-log plot has significant negative slope. The zone of apparently uncorrelated PSD spans a range of spatial scales that are well within the instantaneous field of view (IFOV) of the sensor. In the correlated zone the PSD slope is $\beta = -1.96$ and fractal dimension $H = 0.48$. Because H is close to 0.5, this suggests that the averaged station pass data traces have characteristics that are similar to radiance distributions produced by simple Brownian motion processes.[2]

In Table 1 is presented the latitudinal variation of H within the 1304Å data set. There is a relatively smooth apparent increase in H with latitude, suggesting that there was a possible tendency for the signal to vary less erratically at the higher latitudes than at the lower latitudes. Accompanying the possible latitudinal variation in H are variations in the mean and RMS signal strengths within the 1304 Å data set. This is shown in Table 2. Also included in Table 2 are the mean solar zenith angles for the five latitudinal zones at the times of measurement.

In the uncorrelated zone the PSD has characteristics of white noise, i.e.

$$S_v(\vec{k}) \propto |T(\vec{k})|^2 \; S_w(\vec{k}) \propto S_w(\vec{k}) \tag{2}$$

with $T(\vec{k}) = 1$. The contribution of sensor counting statistics to the power spectral density can be estimated by assuming that the probability of the number of counts k_i in the i^{th} sample period can be described by a Poisson distribution

$$P(K_i) = e^{-M} \frac{M}{K_i 1}^{K_i} \tag{3}$$

where M is the average number of data points in the sample period. The RMS value of the counts is then $\sqrt{M}$. The power spectral density of the sequence of counts is then determined by

$$S_v(\vec{k}) \approx E\left\{ |V_n(\vec{k})|^2 \right\} = \begin{cases} N^2M^2 + NM \text{ for } W = 0 \\ NM \text{ for } W \neq 0 \end{cases} \tag{4}$$

where E is the expectation value for the measured intensities, $\vec{k}$ is spatial frequency, and N is the number of samples used in the discreet Fourier transform. If the variation in the number of counts from sample-to-sample were due primarily to statistical variations in the number of counts due to the count rate being small, i.e., they were dominated by counting statistics, then the power spectral density should have the form expressed in Eq. (4). Normalizing the power spectral density, i.e. $S_v(\vec{k})/S_v(\vec{k} = 0)$, for the Poisson noise model,

$$S_v(\vec{k})/S_v(\vec{k} = 0) \cong 1/NM = 4.7 \times 10^{-5} \tag{5}$$

where $N = 256$ and the mean number of counts is 83 for the data in Figure 1. In the figure the normalized counting variability PSD is plotted with the PSD of the data. It can be concluded from the agreement of the two PSDs that counting noise may have dominated the data in the uncorrelated zone.

Interpretation

The emission at 1304 Å is from the resonant triplet of OI at 1302-4-6 Å [$2p^4 {}^3P_{2,1,0} - 2p^3({}^4S^o)3s^3\ S_1^o$]. The emission arises mainly from the 190 km region and has an overhead rate of $4\pi F \sim 7.5$ kR. Absorption of sunlight from one of the lower levels in the ^3P term can be accompanied by re-emission to another level, making the lines radiatively coupled. Very little O is required to make these resonance transitions optically thick. Furthermore the emissions can be strongly absorbed by O_2, and they can be produced by dissociative excitation of O_2 and photoelectron impact. The result is a complex problem in radiative transfer.

The latitudinal variation in 1304 Å mean intensity may possibly be explained by variations in the resonance scattering phase angle. The phase function for scattering can be represented by a linear combination of the isotropic and Rayleigh phase functions, so that the radial dependence of intensities away from zero solar zenith angle can be approximated by the expression (after Refs. 3 and 4).

$$I \alpha I_o [(\mu + \mu_o)\ \mu_o/\mu]^{1/2} \tag{6}$$

where μ_o and μ are the cosines of the solar zenith angle and spacecraft viewing angles, respectively, and I_o and I are the incident solar and emergent photon fluxes at the top of the atmosphere, respectively. With the spacecraft in nadir viewing orientation, Expression (11) simplifies to

$$I \alpha I_o [(1 + \mu_o)\ \mu_o]^{1/2} \tag{7}$$

In Table 3 derived values of $I/[(1 + \mu_o)\ \mu_o]^{1/2}$ are presented with I from Table 2 (counts). The derived values for $I/[(1 + \mu_o)\mu_o]^{1/2}$ should be proportional to I_o (Expression 12) with no latitudinal dependence. There is, however, a residual latitudinal trend in the results, expressed by the factor A_{lat} in Table 3. A possible origin for the A_{lat} trend is the latitudinal variation in thermospheric temperature. The 1304 Å resonant transitions have large oscillator strengths (f values) and line center absorption cross sections σ_o.[5]

$$\sigma_o = \frac{\pi e^2}{mc} \frac{f}{\Delta \nu_D \sqrt{\pi}} \tag{8}$$

where the line has a Doppler profile with Doppler width given by

$$\Delta\nu_D = \lambda_0^{-1} \sqrt{\frac{2kT}{m(o)}} \quad . \tag{9}$$

Additional temperature dependence occurs for the relative populations of atoms in the three levels of the ^3P ground term

$$p_j = g_j e^{-\Delta E_j/kT} \Big/ \sum_k g_k e^{-\Delta E_k/kT} \tag{10}$$

where j = 2, 1, 0 and where g_j are 5, 3, and 1 for the respective levels $^3P_2$, $^3P_1$, and $^3P_0$.

The latitudinal variation in thermospheric temperature is diurnally and seasonably dependent.[6] With the thermal vertical profile being approximately isothermal over the altitude range of OI emission, the measured intensity of emission should be approximately proportional to $T_\infty^{-1/2}$. In Table 4 the modeled T_∞ for the period of Polar Bear measurements are presented[6] along with $T_\infty^{-1/2}$ normalized to the value for the 20 - 40° latitude zone. A_{lat} is reproduced for comparison. The agreement between normalized $T_\infty^{-1/2}$ and A_{lat} is good for all but the 45 - 65° latitude zone.

The low A_{lat} value for the 45 - 65° latitude zone, if real, suggests the possibility that the source intensity may be reduced by ~5% in that zone. Such a reduction could represent a decrease in source emission intensity and/or an increase in optical absorption by any of several possible magnetospherically-driven processes in this latitude zone. One possibility is that the magnetospherically-driven flow could have induced turbulent mixing that may have resulted in small decreases in the thermospheric O/O_2 and/or O/N_2 mixing ratios in this zone. Small local decreases in [O] could have possibly reduced source emission intensities from either resonance absorption or photoionization processes, depending on altitude. Modifications of O/O_2 or O/N_2 mixing ratios could possibly have affected photoionization production and loss, while small increases in O_2 number density could possibly have locally enhanced optical absorption within this zone. A variety of other magnetospherically driven heating and excitation processes were possible as well, but without independent measurements of the magnetospheric convection electric fields and magnetospheric precipitation at the time of the Polar BEAR measurements, the relative magnitudes of these various processes cannot be directly estimated. A possible clue to the relative significance of these processes, however, comes from the similarity to polar cusp phenomena. The polar cusp occurs close to local noon within the auroral oval, and it takes the form of a sharp decrease in emitted OI intensity at 1304 Å. Northern hemisphere cusps were realistically modeled and discussed by Rees and Fuller-Rowell.[7]

The cusp is produced by a locally enhanced magnetospherically-driven sunward flow, analogous to the proposed possible origin of the mid-latitude effect. In the cusp the enhanced flow produces a local enhancement of temperature and number densities of heavy molecular species (principally O_2 and N_2). It also produces a depletion of atomic oxygen. Temperatures within a modeled Winter northern hemisphere cusp increased by ~6% from 1150°K outside the cusp to 1215°K within the cusp. The modeled atomic oxygen abundance dropped by ~26% from ~27 x 10^{-12} kg m^{-3} to 20 x 10^{-12} kg m^{-3} while the $N_2 + O_2$ density increased by 40% from 10 x 10^{-11} kg m^{-3} to 14 x 10^{-11} kg m^{-3}. Plasma densities tended to decrease within the cusp due to depressed O^+ relative to O_2^+ and NO^+, the latter having higher effective recombination coefficients.

The increases in temperature within the cusp were comparable to those needed to produce the required reduction in oscillator strength; however the sunward velocity change that produced the temperature change was about an order of magnitude greater (several hundred meters per second) than can occur in the mid-latitude zone. At the same time, these winds produced about an order of magnitude greater increase in O_2 number density than required to reduce the oxygen emission by absorption. Reduction in O abundance within the cusp would have reduced the number density of source emitters by a factor of 5 more than observed in the mid latitude effect, neglecting any enhanced absorption by O_2.

Furthermore, the reductions in O and increases of O_2 and N_2 within the cusp acted to reduce plasma densities, accounting in part for the modest 6% increase in temperature produced by several hundred meters per second winds. Within the cusp the reduction in intensity is due primarily to enhanced absorption by O_2, and secondarily to a reduction in the number density of source emitters. The high latitude collisional processes were not as important. In the mid-latitude transition zone it is reasonable to deduce that the observed effect may similarly have been due principally to an increase in O_2 and secondarily to a decrease in O abundance. The relative contribution of the high latitude collisional processes would probably have been even less effective than in the cusp region, due to the substantially lower plasma densities and velocities of magnetospherically driven winds at the mid-latitude transition zone.

In summary, the latitudinal variation in intensity of the Polar Bear 1304 Å data can be reasonably accounted for by resonance scattering and thermospheric temperature models. A small (~5%) deviation from the modeled intensities in the 45 - 65° latitude band, if real, could possibly be attributed to a small decrease in the O/O_2 abundance ratio caused possibly by the expected turbulent reversal in flow direction that occurred at the boundary between anti-sunward solar tidal flow and the sunward magnetospherically-driven flow.

A clue to the origin of the latitudinal variation of H in the 1304 Å data set is their inverse correlation with the average RMS of intensity (counts). The values for H and average RMS are reproduced in Table 5 along with their product H * RMS. The values for H * RMS are generally clustered in the range 3.7 ±0.3. The RMS values are essentially equivalent to the square root of the mean intensity values, and therefore the latitudinal variation in H may possibly be following an $I^{-1/2}$ trend. The possible correlation of H with the mean square root of the mean intensity suggests that the variation in H may possibly have been controlled by continuum scattering. With the principal continuum absorbers being molecular O_2, Rayleigh scattering would be expected to dominate, in which case

$$H * (1 + \cos^2 \theta) = 2 H_o \qquad (11)$$

where H_o is the value of H at $\theta = 0$.

In Table 6 are presented values of $H * (1 + \cos^2 \theta)$ for each latitude zone. For all but the 30 - 50° latitude zone, the results are consistent with a Rayleigh scattering trend with $2 H_o = 0.65 \pm .01$, i.e. with $H_o = .32 - .33$. The value of B_{lat} in Table 6 represents the value of $H * (1 + \cos^2 \theta)$ normalized to $2 H_o$, and it suggests that H in the 30 - 50° latitude zone may have had a significantly higher zero-phase-angle value ($H = 0.38 \pm .03$) than at the other latitudes. The proposal that H = 0.32 - 0.33 (except at 30 - 50°N) when the effects of Rayleigh scattering are removed suggests that the spatial distribution of emitters may be effectively characterized as a scaler Kolmogorov Gaussian field.[8] Mandelbrot[8] investigated the geometric aspects of random fields produced by homogeneous turbulence, based on the Kolmogorov formalism for homogeneous turbulence. It was shown that a zero-mean random Gaussian field, the variance of whose increments obeys the Kolmogorov theory, would be characterized by $\beta = 2H + 1 = 5/3$, or $H = 1/3$. This is in accord with the zero-phase angle value for H (and β) derived here, and it is consistent with a spatial morphology of intensity (with the effects of scattering removed) that is possibly controlled predominantly by

turbulent processes. The turbulence field, like the ideal fractal Brownian field, is isotropic and it has no intrinsic scale, i.e. large and medium scale morphology is essentially the same as the morphology at fine spatial scales, in the spatial scale ranges where other non-turbulent processes or cut-offs do not affect the distribution.

If, as proposed, Rayleigh scattering was the dominant cause of the increased H, then the principal effect would have been the preferential suppression of fine-scale morphology, rather than an enhancement of coarse-scale morphology. The process acts to scatter photons from zones of relatively high source intensity into zones of relatively low intensity, reducing intensity contrast, i.e. suppressing apparent morphology. Because of the finite mean free paths of the photons, the extent of contrast reduction is greatest for closely-spaced contrast features, hence the probable preferential suppression of fine-scale morphology and resultant increased H.

While Rayleigh scattering appears to possibly account for most of the latitudinal variation in H, the values of B_{lat} in Table 6 reveal that there may have been an additional contribution from another process in the 30 - 50° latitude zone. In that zone the value of H appears to have been possibly increased by an additional ~17% by some process that may have either preferentially suppressed fine-scale morphology or preferentially enhanced coarse-scale morphology, or both. A possibility is that there may have been enhanced dissipation of fine-scale morphology arising from ion drag shear in the latitude zone. In the 30 - 50° latitude zone there can be large variations in ion-neutral difference velocities and therefore large differences in ion drag shear forces.[9] The rapid fluctuation of drag shear forces would tend to preferentially disrupt fine-scale morphology. In particular, dissipation of large scale morphology occurs by viscous coupling to the smaller scale turbulence. The momentum transfer to the larger features is sluggish relative to the rapidly varying ion convection speeds and directions, due both to the relatively long time constants for momentum coupling (~10^2 minutes) and the dependence of the momentum coupling on the local ion density, which is extremely variable in this latitude zone. The result would probably be a preferential dissipation of fine-scale morphology.

While H was derived from data that spanned the 30 - 1400 km spatial scale range, the range is not limiting. The lower limit of the spatial scale range was imposed by the sensor and not the background. The upper limit was constrained by the volume of data that could be handled by the computer. If, as proposed, the derived values of H were controlled primarily by turbulence and Rayleigh scattering, the range of spatial scales over which H was valid could possibly be significantly larger than 30 - 1400 km. In the inertial subrange, where the Kolmogorov power law is strictly valid, the low-wavenumber limit is theoretically the reciprocal of the vertical distance to the nearest stable layer.[10] This would be approximately 10^5 meters. Observations indicate that the power law is valid well beyond that limit even in highly stratified conditions.[10] In the thermospheric regime, where stratification is less pronounced, the power law may be valid up to the scales of solar forcing (~10^7 meters). The Polar BEAR data appears to obey the power law at scales of ~10^6 meters, and hence a low wavenumber limit of 10^6 - 10^7 meters is probably reasonable. The upper limit of the Kolmogorov power law spatial frequency range is theoretically defined as the Kolmogorov microscale. Above the turbopause, however, where viscosity effects can

be considered unimportant, eddy scales will be limited by the mean free path. With emissions emanating primarily from the 170 - 400 km elevation range, the mean free path (U.S. Standard Atmosphere) is 10^2 - 10^3 meters. At scales finer than 10^2 - 10^3 meters, the loss of eddy structure will result in a steeper power spectral density slope (more negative β).

Except for the mid-latitude transition zone and the auroral oval, therefore, it is reasonable to assume that the range of spatial scales over which he derived values of β may be characteristic spans from a fine-scale cut-off of ~10^2 - 10^3 meters to a coarse-scale cut-off of ~10^6 - 10^7 meters. At scales finer than 10^2 - 10^3 meters, β should become more negative. The β value for the mid-latitude transition zone, where it is proposed that turbulence is possibly suppressed by drag shear, may represent a reasonable approximation to the value of β in the range of the fine-scale cut-off. Mandelbrot[8] suggested that the characteristic turbulence value for H may extend beyond the Kolmogorov microscale limit; consequently it is reasonable that β may possibly gradually become more negative, rather than sharply change, near 10^2 - 10^3 meters. If it is assumed that the β and H near the fine scale cut-off have values comparable to the derived values for the mid-latitude transition zone, where turbulence is sheared-off, then the zero phase angle value for H may gradually increase from H = 0.33 at ~10^3 meter scales to H ≈ 0.4 at finer scales. Similarly, at scales coarser than 10^6 - 10^7 meters, β should become gradually less negative, reflecting a suppression of coarse scale structure.

Summary

The results reported here suggest that the spatial radiance characteristics of the ultraviolet earth background of the 1304 Å are generally consistent with current understanding of the underlying phenomenology. The analysis emphasized dayside radiance during northern summer at 20 - 90° latitudes. For those conditions at least it appears that the spatial characteristics of the background, measured by a nadir-viewing space-based sensor, can probably be modeled with good radiometric integrity over a relatively broad range of spatial scales. The spatial structure may be controlled principally by turbulence over spatial scales of 10^7 - 10^2 meters, with modifications imposed by Rayleigh scattering effects and magnetospherically forced phenomena. Spatial structure can be modeled fractally, using dimensions based on Kolmogorov formalism modified by the Rayleigh scattering phase function. Mean radiance can be modeled using current parametric expressions of radiant intensity, resonance scattering, and absorption combined with the thermospheric compositional and general circulation models, such as MSIS-83, scaled to the mean and RMS intensities measured by Polar BEAR.

An estimation of spatial clutter as measured by a nadir-viewing space-based sensor at fine spatial scales, based on the results of the analysis here, is presented in a companion paper.[1]

2. ACKNOWLEDGMENTS

This research was supported by Air Force Contract Numbers F19628-87-C-0206 and F19628-89-C-0091 from the UV Surveillance and Remote Sensing Branch, Ionospheric Research Division, Air Force Geophysics Laboratory, Hanscom AFB, MA.

3. REFERENCES

1. R. Wohlers, R. Huguenin and M. Weinberg, "Estimated UV Clutter Levels at 10-100 Meter Sensor Pixel Resolution Extrapolated From Recent Polar Bear Measurements," SPIE (this volume), 1989.

2. R.F. Voss, Fractals in Nature: From Characterization to Simulation, in H.O. Pertgen and D. Saupe, eds. "The Science of Fractal Images," Springer-Verlag, New York, 21-70, 1988.

3. D.J. Strickland, G.E. Thomas and P.R. Sparks, "Mariner 6 and 7 Ultraviolet Spectrometer Experiment: Analysis of the OI 1304 - and 1356 Å Emissions," J. Geophys. Res. 77, 4052-4061, 1972.

4. D.J. Strickland, "The OI 1304- and 1356 Å Emissions from the Atmosphere of Venus," J. Geophys. Res., 78, 2827-2836, 1973.

5. D.J. Strickland and T.M. Donahue, "Excitation and Radiative Transport of OI 1304 Å Resonance Radiation - I. The Dayglow," Planet. Space Sci., 18, 661-689, 1970.

6. A.E. Hedin, "A Revised Thermospheric Model Based on Mass Spectrometer and Inchoerent Scatter Data: MSIS-83," J. Geophys. Res., 88, 10170-10179, 1983.

7. D. Rees and T.J. Fuller-Rowell, "A Theoretical Thermosphere Model for CIRA, Adances Space Research, 1, 185-198, 1987.

8. B.B. Mandelbrot, "On the Geometry of Homogeneous Turbulence, With Stress on the Fractal Dimension of the Isosurfaces of Scalars," J. Fluid Mech., 72, 401-416, 1975.

9. T.L. Killeen, T.L. Craven, L.A. Frank, J.J. Ponthieu, N.W. Spencer, R.A. Heelis, L.H. Brace, R.G. Roble P.B. Hays and G.R. Carignam, "On the Relationship Between Dynamics and Polar Thermosphere and Morphology of the Aurora: Global-Scale Observations from Dynamics Explorers 1 and 2," J. Geophys. Res., 93, 2675-2692, 1988.

10. J.L. Lumley and H.A. Panofsky, "The Structure of Atmospheric Turbulence," Interscience, New York, Chapter 5, 1964.

Table 1 - Latitudinal Characteristics of the 1304 Å Data

LAT (°N)	-β	H
20 - 40	-1.75 ±0.09	0.38 ±0.04
30 - 50	-1.91 ±0.04	0.46 ±0.02
45 - 65	-1.91 ±0.18	0.46 ±0.09
60 - 75	-1.97 ±0.01	0.49 ±0.01
70 - 89	-2.08 ±0.08	0.54 ±0.04

Table 2 - Latitudinal Characteristics of the 1304 Å Data (Cont'd)

LAT (°N)	Mean (Counts)	RMS (Counts)	Solar Zenith Angle (deg)
20 - 40	80.0	9.0	32.0
30 - 50	76.1	8.8	36.2
45 - 65	64.1	8.3	45.8
60 - 75	57.5	7.8	54.9
70 - 89	47.0	6.9	64.7

Table 3 - Resonance Scattering Phase Angle

Latitude Zone	μ_o	$I/[(1 + \mu_o)\ \mu_o]^{1/2}$	A_{lat}
20 - 40	0.848	63.9	1.00
30 - 50	0.806	63.1	0.99
45 - 65	0.697	59.0	0.92
60 - 75	0.575	60.4	0.95
70 - 89	0.427	60.2	0.94

Table 4 - Modeled Thermospheric Temperatures

Latitude (°N)	T_∞ (°K)	$T_\infty^{-1/2}$, Normalized	A_{lat}	$A_{lat}/T_\infty^{-1/2}$, Normalized
20 - 40	1100	1.00	1.00	1.00
30 - 50	1125	0.99	0.99	1.00
45 - 65	1160	0.97	0.92	0.95
60 - 75	1215	0.95	0.95	1.00
70 -84	1235	0.94	0.94	1.00

Table 5 - Inverse Correlation of H and RMS

Δlat	H	RMS	H * RMS
20 - 40	0.38 ±0.04	9.0	3.42 ±0.36
30 - 50	0.46 ±0.02	8.8	4.04 ±0.17
45 - 65	0.46 ±0.09	8.3	3.82 ±0.74
60 - 75	0.49 ±0.01	7.8	3.82 ±0.39
70 - 89	0.54 ±0.04	6.9	3.73 ±0.28

Table 6 - Inverse Correlation of H and Rayleigh Scattering Phase Function

Δlat	H	$(1 + \cos^2 \Theta)$	H * $(1 + \cos^2 \Theta)$	B_{lat}
20 - 40	0.38 ±0.04	1.720	0.65 ±0.07	1.00 ±0.13
30 - 50	0.46 ±0.02	1.651	0.76 ±0.03	1.17 ±0.06
45 - 65	0.46 ±0.09	1.482	0.68 ±0.13	1.05 ±0.22
60 - 75	0.49 ±0.01	1.331	0.65 ±0.01	1.00 ±0.03
70 - 89	0.54 ±0.04	1.182	0.64 ±0.05	0.99 ±0.10

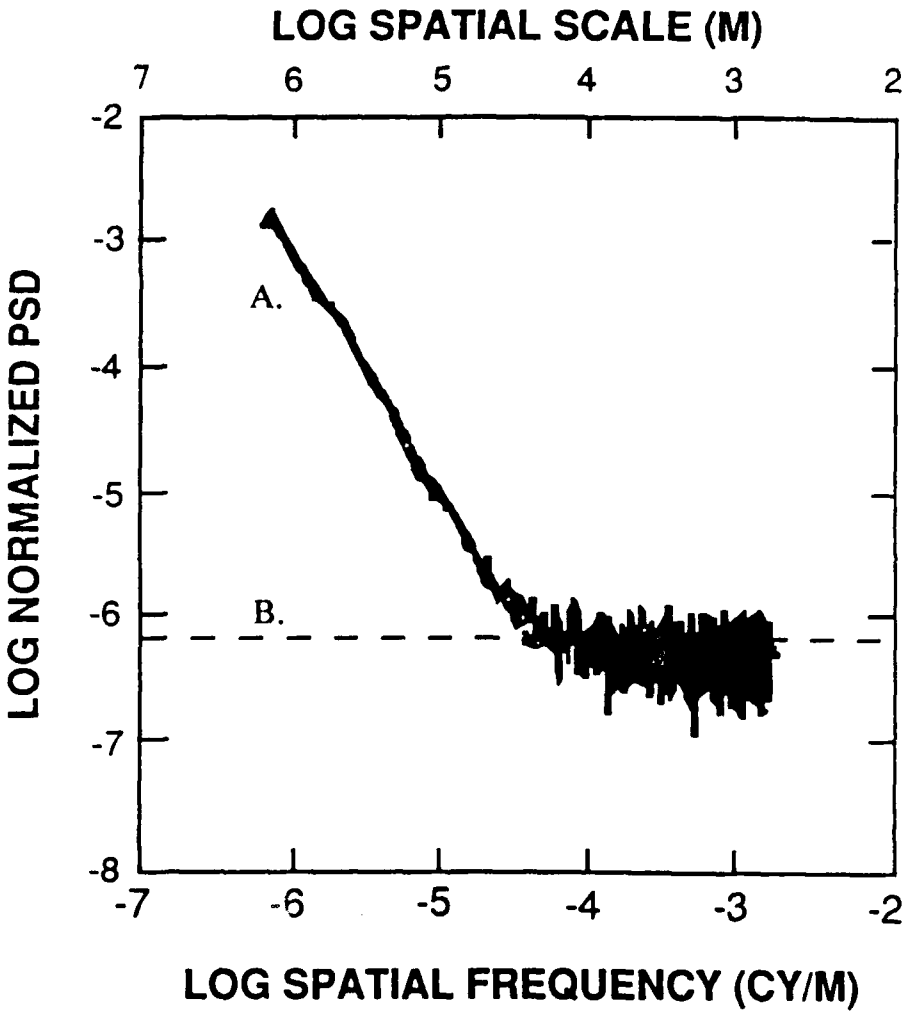

Fig. 1. (a) Average of 15 PSDs of 1304 Å data. (b) Counting statistics PSD